applied sciences

MDPI

Article

Research on Multiscale Simulation Methods for Thermal Response of Cemented Sand–Gravel Dams

Ling Zhong [1,2,†], Ying Zhang [1,*,†], Lixia Guo [1,2] and Jianwei Zhang [1]

[1] School of Water Conservancy, North China University of Water Resources and Electric Power, Zhengzhou 450046, China; zhongling@ncwu.edu.cn (L.Z.); guolixia@ncwu.edu.cn (L.G.); zhangjianwei@ncwu.edu.cn (J.Z.)
[2] Henan Key Laboratory of Water Environment Simulation and Treatment, Zhengzhou 450002, China
* Correspondence: z20241010075@stu.ncwu.edu.cn
† These authors contributed equally to this work.

Abstract

Cemented sand and gravel (CSG) dams have been widely applied due to their simple construction and use of local materials. With the increasing occurrence of extreme weather events, temperature has become an important factor affecting the safe operation of dams. To investigate the temperature stress response of CSG dams under low-temperature conditions and achieve cross-scale analysis, an adaptive macro–meso finite element method is proposed. Through an iterative "solution–evaluation–mesh adjustment" procedure, meso-scale modeling is performed in high-stress regions, and the results are compared with those obtained using the conventional submodeling method. The results show that, under low-temperature conditions, temperature gradients and thermal stresses are mainly concentrated near the dam surface, with limited influence on the interior, while hydraulic load remains the dominant controlling factor. The local stress distribution patterns obtained by the two methods are generally consistent, and both can reflect stress concentration near the aggregate–mortar interfaces. The proposed method can characterize local meso-scale responses within a global computational framework, providing a reference for cross-scale analysis of the temperature response and the identification of local unfavorable stress regions in CSG dams.

Keywords: cemented sand–gravel dam; thermal stress; multiscale computation; adaptive macro-meso finite element method

1. Introduction

Cemented sand and gravel (CSG), as a novel dam construction material composed of natural sand–gravel aggregates and a small amount of cementitious materials, has gradually emerged as a promising green material in hydraulic engineering due to its advantages of low cost, low carbon emissions, convenient construction, and adaptability to complex foundations [1–3]. However, in recent years, with the increasing occurrence of extreme weather events, CSG dams in operation are subjected to combined effects of ambient temperature variations, reservoir water temperature stratification, and freezing conditions. These factors tend to induce significant temperature gradients near the dam surface and in locally constrained regions, which may further generate unfavorable thermal stresses [4,5], thereby affecting the local stress state and long-term operational performance of the dam. At present, most studies on CSG dams focus on their macroscopic performance during the construction stage, while investigations on response mechanisms under environmental

Academic Editor: Paulo Santos

Received: 13 May 2026
Revised: 27 June 2026
Accepted: 29 June 2026
Published: 5 July 2026

effects during the operational stage—especially cross-scale studies integrating macro- and meso-scale analyses—remain relatively limited. Therefore, conducting cross-scale temperature response analysis of CSG dams during operation is of great significance for revealing local unfavorable stress characteristics and understanding their thermo-mechanical response under low-temperature conditions.

To balance the computational efficiency of macro-scale models and the physical accuracy of meso-scale models, adaptive multiscale finite element methods have become an effective approach. Such methods typically perform meso-scale refinement in critical local regions of macro models based on structural response states, thereby achieving a compromise between computational cost and accuracy. Existing studies mainly focus on two aspects: (i) the establishment of adaptive criteria and execution mechanisms, and (ii) the construction of meso-scale models and their coupling with macro-scale regions. For the former, stress or damage indicators are commonly used as triggering criteria for scale transition. For instance, Rodrigues et al. [6] identified potential damage zones using macro-scale stress fields and embedded meso-scale models consisting of aggregates, mortar, and interfacial transition zones, ensuring displacement compatibility across non-matching meshes. Sun and Li [7] employed damage evolution as an adaptive criterion and developed a multigrid finite element method, enabling efficient simulation from material damage to structural failure through dynamic mesh refinement. To further improve computational efficiency, hierarchical and multi-level strategies have been proposed. Sun and Li [8] introduced a damage-based adaptive three-level model, while Lei et al. [9] and Xu Lei et al. [10] developed a "macro integration point–meso sample" coupling approach, in which meso-scale models are generated at critical points, reducing computational cost to 17.57% of full-field meso-scale simulation and significantly improving efficiency in cross-scale damage analysis.

Regarding meso-scale model construction and coupling, existing research mainly aims to balance the representation of material heterogeneity and numerical stability. Unger and Eckardt [11] established a representative meso-scale model based on randomly distributed ellipsoidal aggregates and proposed a coupling framework with macro-scale fields. Rezakhani et al. [12] further proposed an adaptive multiscale homogenization method, in which the macroscopic failure criterion is directly calibrated by meso-scale discrete particle models, enabling high-fidelity meso-scale analysis to be activated only in necessary local regions.

In summary, current studies have formed a methodological framework represented by multiscale damage simulation of structures [13]. However, most research focuses on conventional concrete materials, and cross-scale studies on the temperature response of CSG dams during operation remain insufficient. In addition, local meso-scale regions in many studies are predefined, making it difficult to adaptively identify and refine unfavorable regions based on structural response. On this basis, a local macro–meso transition analysis method is developed within the adaptive macro–meso finite element framework for the thermo-mechanical response of CSG dams during operation. The method employs a principal tensile stress threshold as the triggering criterion for local scale transition and integrates the embedding of random polygonal–aggregate meso-scale models, compatible mesh reconstruction, and the unified stiffness assembly and solution of macro- and meso-scale elements, thereby enabling cross-scale simulation of the thermo-mechanical response of CSG dams.

Starting from the finite element model, the multiscale finite element model is established and solved through a "solution–evaluation–mesh adjustment" procedure. The distributions of the temperature and stress fields in a CSG dam under extreme low-temperature conditions are investigated, and the meso-scale stress response characteristics of local

regions are further analyzed. The results provide a reference for cross-scale temperature response analysis and the identification of local unfavorable stress regions in CSG dams operating in cold regions.

2. Computational Method and Model Setup

2.1. Thermo-Mechanical Coupling Theory

In the analysis of the loading behavior of cemented sand and gravel (CSG) dams during construction and operation under temperature effects, the transient temperature field of the dam is governed by the law of energy conservation and Fourier's law of heat conduction. The governing equation can be expressed as Equation (1) [14]:

$$\rho c \frac{\partial T}{\partial t} = \nabla \cdot (k \nabla T) + Q \tag{1}$$

where ρ is material density (kg/m^3), c is the specific heat capacity (J/(kg·°C)), T is the temperature (°C), t is time (s), k is the thermal conductivity (W/(m·°C)), and Q is the internal heat source intensity (W/m^3).

The corresponding initial and boundary conditions for the heat conduction problem can be expressed as Equations (2)–(5):

$$T(x, 0) = T_0(x), x \in \Omega \tag{2}$$

$$T = \bar{T}, x \in \Gamma_T \tag{3}$$

$$-k \nabla T \cdot n = \bar{q}, x \in \Gamma_q \tag{4}$$

$$-k \nabla T \cdot n = h_c (T - T_a), x \in \Gamma_h \tag{5}$$

where x is the spatial coordinate vector, Ω is the computational domain, T_0 is the initial temperature, T is the prescribed temperature, $\bar{q}$ is the prescribed heat flux, n is the outward normal vector, h_c is the convective heat transfer coefficient, T_a is the ambient temperature, and Γ_T, Γ_q, and Γ_h denote the prescribed temperature boundary, heat flux boundary, and convective boundary, respectively.

In CSG dams, the internal heat source Q mainly originates from cement hydration. The heat release process is commonly described using an adiabatic temperature rise model. Let $\theta(t)$ denote the adiabatic temperature rise caused by hydration heat under adiabatic conditions.

$$Q = \rho c \frac{d\theta}{dt} \tag{6}$$

Substituting this into Equation (1) and defining the thermal diffusivity $\alpha = \frac{k}{\rho c}$, the governing equation can be rewritten accordingly:

$$\frac{\partial T}{\partial t} = \alpha \nabla^2 T + \frac{\partial \theta}{\partial t} \tag{7}$$

where $\nabla^2 = \frac{\partial^2}{\partial x^2} + \frac{\partial^2}{\partial y^2} + \frac{\partial^2}{\partial z^2}$. Substituting Equation (7) into Equation (6) yields the following:

$$\frac{\partial T}{\partial t} = \alpha \left(\frac{\partial^2 T}{\partial x^2} + \frac{\partial^2 T}{\partial y^2} + \frac{\partial^2 T}{\partial z^2} \right) + \frac{\partial \theta}{\partial t} \tag{8}$$

Temperature variations induce thermal strain in CSG materials, which in turn generate thermal stress. Referring to previous simulation studies on freeze–thaw damage in hydraulic concrete structures [15], the possible frost heave deformation under low-temperature conditions is equivalently represented by the temperature–strain term in this

study and introduced into the stress analysis through the temperature–strain increment. According to elasticity theory, the relationship between thermal strain ε^T and temperature change ΔT [16] is as follows:

$$\varepsilon^T = \alpha \Delta T \tag{9}$$

where α is the coefficient of thermal expansion. In the finite element incremental calculation, the temperature–strain increment can be expressed as follows:

$$\left\{\Delta \varepsilon_n^T\right\} = \{\alpha \Delta T_n, \alpha \Delta T_n, \alpha \Delta T_n, 0, 0, 0\} \tag{10}$$

where $\Delta \varepsilon_n^T$ is the temperature–strain increment, and ΔT_n is the temperature increment in the corresponding time step. When the temperatures in two consecutive time steps are below 0 °C, the possible frost heave deformation of concrete is equivalently treated as a special case of thermal expansion and contraction, and a negative linear expansion coefficient is adopted.

Based on Hooke's law, the stress–strain relationship considering thermal strain can be written as follows:

$$\sigma_{ij} = C_{ijkl}\left(\varepsilon_{kl} - \varepsilon_{kl}^T\right) \tag{11}$$

where σ_{ij} is the stress tensor, C_{ijkl} is the elastic stiffness tensor, and ε_{kl} is the total strain tensor.

The elastic boundary-value problem of the dam can be expressed as follows:

$$\sigma_{ij,j} + b_i = 0, x \in \Omega \tag{12}$$

$$u_i = \bar{u}_i, x \in \Gamma_u \tag{13}$$

$$\sigma_{ij} n_j = \bar{t}_i, x \in \Gamma_t \tag{14}$$

where b_i is the body-force component, u_i is the displacement component, $\bar{u}_i$ is the prescribed displacement, n_j is the component of the outward normal vector, $\bar{t}_i$ is the prescribed boundary component, and Γ_u and Γ_t denote the displacement boundary and traction boundary, respectively. The comma in the subscript denotes partial differentiation with respect to the spatial coordinate, and repeated indices follow the Einstein summation convention.

In this study, a sequential coupling approach is adopted for thermos-mechanical analysis. First, the temperature field of the dam is solved, and the resulting temperature increments are converted into thermal strains and applied to the mechanical model to obtain the corresponding thermal stress distribution [17,18]. Subsequently, the principal tensile stress is used to determine whether local regions satisfy the criteria for meso-scale substitution, followed by macro–meso transition analysis. It should be noted that this study focuses on local stress concentration induced by temperature fields during low-temperature operation. Therefore, both thermal and mechanical parameters are assumed to be constant, and the bidirectional strong coupling effects—such as the influence of stress on thermal conductivity and specific heat—are neglected.

2.2. Adaptive Macro–Meso Finite Element Method

Starting from the finite element model, the multiscale finite element model is established and solved through a "solution–evaluation–mesh adjustment" procedure. The distributions of the temperature and stress fields in a CSG dam under extreme low-temperature conditions are investigated, and the meso-scale stress response characteristics of local regions are further analyzed. The results provide a reference for the crack-resistant design and safety assessment of CSG dams operating in cold regions. In the coupled temperature–

stress analysis of CSG dams, to accurately capture local stress concentrations induced by temperature effects while maintaining overall computational efficiency, a local macro–meso transition analysis method is developed within the adaptive macro–meso finite element framework for the operational thermo-mechanical response of CSG dams. Through the "solution–evaluation–mesh adjustment" procedure [19], local high-stress regions are identified according to the principal tensile stress response of the macro-scale model, and the macro-scale elements satisfying the triggering criterion are subjected to meso-scale substitution analysis.

The complete multiscale model consists of macro-scale elements and local meso-scale elements, which describe material behavior at different scales. At the macro scale, the dam body is treated as a homogeneous material and modeled using a linear elastic constitutive relationship to represent the global mechanical response. At the meso scale, the material is explicitly represented by aggregates and mortar, both assumed to follow linear elastic behavior [20,21]. The macro model captures the overall structural response, while the meso model characterizes stress redistribution caused by material heterogeneity. The present study focuses on the stress response in the pre-cracking elastic stage and does not consider nonlinear behavior such as crack initiation, crack propagation, or interface debonding.

According to Ref. [11], when the principal tensile stress at any integration point within a macro element exceeds a prescribed threshold, and the element corresponds to CSG material, a local adaptive adjustment is triggered. Specifically, the macro element is replaced by a meso-scale model with randomly distributed aggregates, and local mesh compatibility is ensured through coordinated remeshing. This enables deformation compatibility between macro and meso domains, allowing both scales to participate in the global stiffness matrix assembly.

In this study, a principal tensile stress threshold of 0.15 MPa is adopted as the criterion for triggering local meso-scale analysis to identify unfavorable stress regions in the dam, and its basis is further discussed in Section 4.1. It should be noted that this threshold is not intended to serve as a macroscopic cracking criterion. Since the selected value is lower than the splitting tensile strength of the CSG material, it is used only as an adaptive indicator to identify potentially unfavorable high-tensile-stress regions or stress-concentration zones requiring further meso-scale analysis. In contrast, the identification of macroscopic cracking would require the tensile stress to reach or exceed the material tensile strength and should generally be further supported by damage evolution or crack propagation criteria. Therefore, the refined regions in this study should be interpreted as local stress-concentration regions rather than regions where macroscopic cracking has already occurred.

The meso-scale model is constructed as follows [10]: First, nodal information of the damaged macro element and the associated integration point area or volume are obtained to determine the size of the meso model. Based on parameters such as aggregate volume fraction, particle size distribution, and gradation, crushed stone aggregates are idealized as irregular polygons. Random circular inclusions are generated, within which quadrant partitioning is performed to define the number and coordinates of vertices. These vertices are then connected to form polygonal aggregates [22,23]. The regions not occupied by aggregates are defined as the mortar matrix, thereby forming a single random polygonal-aggregate meso-scale model within the target element satisfying the principal tensile stress threshold.

During the numerical implementation, when multiple elements simultaneously satisfy the stress criterion, the maximum first principal tensile stresses at the integration points of the candidate elements are compared, and the element with the largest value is selected for meso-scale substitution to represent the most critical local mechanical response within

the candidate region. The selected element is subsequently used for the corresponding comparison with the submodeling method.

Based on the above procedure, the core workflow of the proposed adaptive multiscale modeling strategy is illustrated in Figure 1. Figure 1a shows the model substitution process triggered by the stress threshold. Specifically, the macro-scale stress field is first evaluated, and the CSG macro element satisfying the prescribed principal tensile stress threshold is selected for meso-scale substitution. Figure 1b shows the coordinated mesh discretization after local substitution. The selected macro-scale region is replaced by a meso-scale model composed of aggregates and mortar, while the surrounding mesh is adjusted to ensure deformation compatibility at the macro–meso interface.

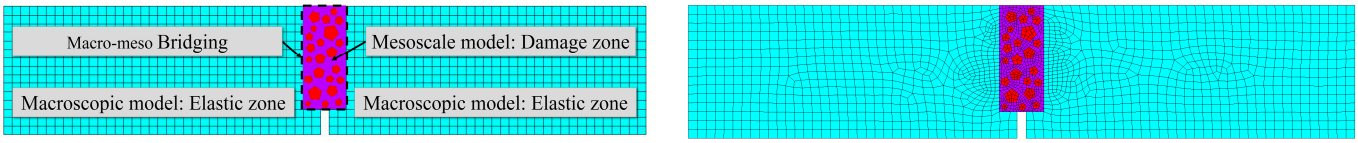

(**a**) Stress-threshold-triggered model substitution (**b**) Mesh compatibility remeshing in local regions

Figure 1. Adaptive model substitution and mesh compatibility remeshing. The cyan region represents the macroscopic elastic zone, while the purple mortar matrix and red aggregates together constitute the mesoscale damage zone.

The proposed adaptive macro–meso finite element method (FEM) performs meso-scale substitution only in locally unfavorable regions based on the macro-scale analysis. Since the substituted regions are relatively small compared to the entire structure, their influence on the global thermal stress distribution is limited, and the method is primarily intended to characterize local meso-scale mechanical responses. Compared with full meso-scale simulations, the proposed approach significantly reduces computational cost. Moreover, in contrast to conventional local methods with predefined analysis regions, this method can identify critical high-stress zones based on the actual structural response of the dam and subsequently conduct targeted meso-scale analysis.

2.3. Submodel Method

Submodeling techniques are based on Saint-Venant's principle and focus on critical regions of a structure that require detailed analysis. These regions are extracted from the global model and discretized with refined meshes to obtain accurate local responses [24–27].

According to finite element theory, any structural system satisfies the following equilibrium equation:

$$[\boldsymbol{K}]\{\boldsymbol{U}\} = \{\boldsymbol{F}\} \tag{15}$$

where $[\boldsymbol{K}]$ is the global stiffness matrix, $\{\boldsymbol{U}\}$ is the displacement vector, and $\{\boldsymbol{F}\}$ is the load vector.

Assuming that the global model consists of two parts, denoted as substructure I and substructure B, the displacement vector can be partitioned into $\boldsymbol{U}_{\mathrm{I}}$ and $\boldsymbol{U}_{\mathrm{B}}$. If $\boldsymbol{U}_{\mathrm{B}}$ is known, Equation (15) can be rewritten as follows:

$$\begin{bmatrix} \boldsymbol{K}_{\mathrm{II}} & \boldsymbol{K}_{\mathrm{BB}} \\ \boldsymbol{K}_{\mathrm{BI}} & \boldsymbol{K}_{\mathrm{BB}} \end{bmatrix} \begin{Bmatrix} \boldsymbol{U}_{\mathrm{I}} \\ \boldsymbol{U}_{\mathrm{B}} \end{Bmatrix} = \begin{Bmatrix} \boldsymbol{F}_{\mathrm{I}} \\ \boldsymbol{F}_{\mathrm{B}} \end{Bmatrix} \tag{16}$$

where $\boldsymbol{K}_{\mathrm{II}}$ and $\boldsymbol{K}_{\mathrm{BB}}$ are the stiffness matrices of substructures I and B, respectively; $\boldsymbol{U}_{\mathrm{I}}$ and $\boldsymbol{U}_{\mathrm{B}}$ are the corresponding displacement vectors; and $\boldsymbol{F}_{\mathrm{I}}$ and $\boldsymbol{F}_{\mathrm{B}}$ are the corresponding load vectors.

Equation (16) can be further reduced to the following:

$$[K_{II}]\{U_I\} = \{F_I\} - [K_{IB}]\{U_B\} \quad (17)$$

Equation (17) represents the theoretical basis of the submodeling method. It indicates that, under certain conditions, for structures with stiffness, displacement boundary conditions can be equivalently transformed into load vectors. In other words, imposed displacement constraints will generate corresponding load effects, which can be applied to the submodel for local analysis.

2.4. Finite Element Model, Material Parameters, and Boundary Conditions

In this study, the Shoukoubao cemented sand and gravel (CSG) dam was selected as the engineering case for a multiscale numerical analysis of its thermal response. The Shoukoubao dam, located in Yanggao County, Shanxi Province, China, is a completed and operating CSG dam. The prototype dam adopts a full-section composite structure consisting of an inner CSG dam body and outer concrete layers. A representative central section of the dam was selected, and a two-dimensional plane-strain finite element model was established. This assumption was adopted because the geometry, material zoning, and principal loads vary only slightly along the dam axis direction within the investigated section. The computational model of the typical cross-section is shown in Figure 2. The dam has a crest width of 6 m, a height of 60 m, and a base width of 78 m. The upstream and downstream concrete facings are both 1 m thick. The concrete bedding layer is 198 m wide and 1 m thick, while the foundation is 198 m wide and 59 m deep. The initial finite element model is a macro-scale model consisting of four material regions: the central CSG dam body, the concrete facings, the concrete bedding layer, and the granite bedrock. Model construction, mesh generation, and the subsequent thermal and mechanical analyses were performed using ANSYS Mechanical APDL 2022 R2. A sequentially coupled thermo-mechanical analysis was adopted, in which the temperature field was first calculated and then transferred to the structural model as a thermal load for the stress analysis.

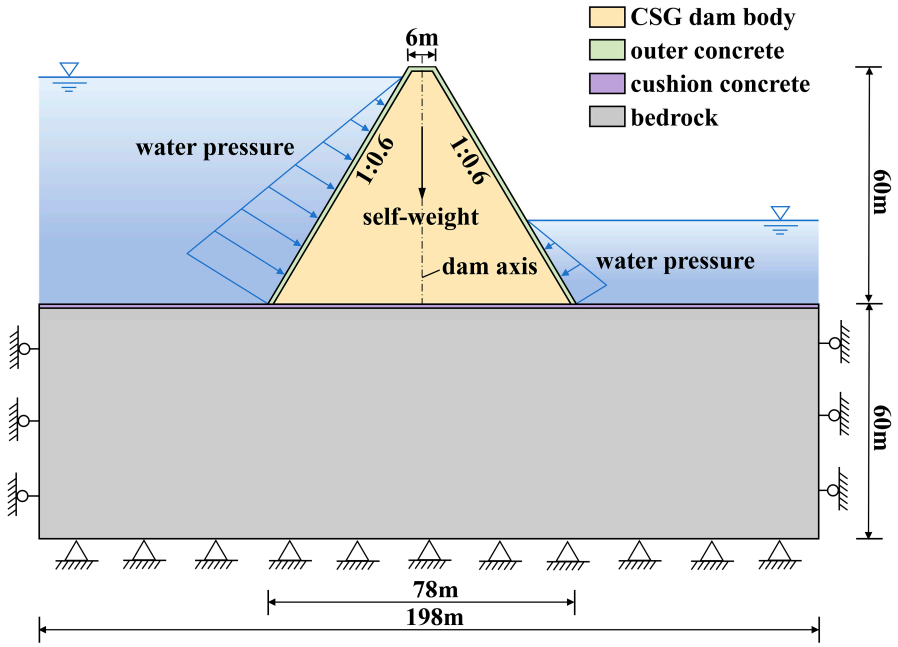

Figure 2. Schematic of the standard-section computational model.

To clearly illustrate the mesh discretization characteristics of the finite element model, a simplified finite element mesh is presented in Figure 3. In this schematic model, the longer geometric edges are divided into 20 segments, whereas the shorter edges are divided into two segments. This simplified mesh is used only to provide an intuitive representation of the mesh distribution. A finer mesh is adopted in the actual numerical analysis, in which the corresponding longer edges are divided into 80 segments and the shorter edges into two segments. The actual finite element model contains 26,896 elements and 27,305 nodes.

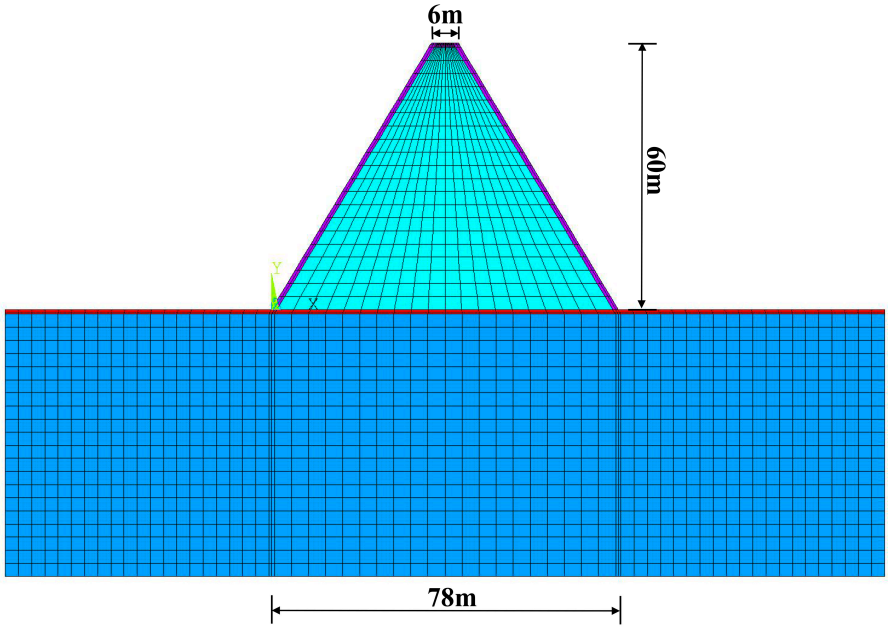

Figure 3. Schematic of finite element model. The cyan region represents the CSG dam body, the purple regions represent the outer concrete layers, the red region represents the cushion concrete, and the blue region represents the bedrock.

To examine the adequacy of the selected mesh, a mesh-dependence check was further conducted. In the calculation, only the mesh density was varied, while the material parameters, boundary conditions, and loading conditions were kept unchanged. As shown in Table 1, with mesh refinement, the maximum principal tensile stress near the upstream dam heel gradually tends to stabilize, and the location of the high-tensile-stress region remains consistent. Therefore, the adopted mesh can satisfy the accuracy requirements of the present numerical analysis and is used for the subsequent local meso-scale analysis.

Table 1. Comparison of the maximum principal tensile stress under different mesh densities.

Mesh Type	Long-Edge Divisions	Short-Edge Divisions	Number of Elements	Number of Nodes	Maximum Principal Tensile Stress (MPa)
Coarse mesh	40	2	7056	7265	0.52
Adopted mesh	80	2	26,896	27,305	0.60
Fine mesh	120	2	62,010	62,617	0.64

At the macro scale, all materials are modeled using a linear elastic constitutive model. The thermal and mechanical parameters are determined based on the relevant literature and previous studies of the Shoukoubao dam [28,29]. The material parameters of the dam are listed in Table 2. All material interfaces in the macro- and meso-scale models are assumed to be perfectly bonded, with continuous displacement and temperature across the interfaces. Interfacial slip, debonding, and damage are not considered.

Table 2. Computational parameters of model.

Model	Material	Elastic Modulus (GPa)	Poisson's Ratio	Thermal Conductivity (W/(m·K))	Specific Heat Capacity (J/(kg·°C))	Coefficient of Linear Thermal Expansion (10^{-6}/°C)
Macroscopic model	Outer concrete layer	27	0.20	2.31	1100	6.80
	CSG (dam body)	10	0.20	2.15	990	5.60
	Cushion concrete	20	0.20	2.72	1090	6.92
	Bedrock	25	0.25	2.50	880	5.00
Mesoscopic model	Mortar	8	0.22	1.50	950	10.00
	Aggregate	50	0.25	2.80	850	5.00

The temperature field calculation adopts a non-uniform temperature distribution that has stabilized after long-term reservoir operation as the initial condition. To investigate the effects of extreme weather, the low-temperature operating condition in January is selected as the representative scenario. Temperature boundary conditions are applied according to the environmental zones of the dam surface. For the dam surface above the water level and directly exposed to air, a temperature boundary combining the winter monthly average air temperature and solar radiation-induced temperature rise is adopted, with a representative ambient temperature of −8 °C. For the upstream dam surface in contact with reservoir water, a depth-dependent water temperature distribution is applied. Based on the thermal equilibrium principle at the ice–water interface, the surface ice layer isolates heat exchange between cold air and the underlying water, maintaining the temperature beneath the ice near the freezing point, which is taken as 0.8 °C. This treatment reasonably reflects the non-uniform temperature distribution characteristics of the dam surface under the combined influence of cold air and relatively warm reservoir water during cold seasons. The depth-dependent reservoir-water temperature is estimated using Equation (18). This equation is adapted from the mean-temperature component of Zhu's empirical deep-reservoir water temperature model [30] to the representative January operating condition considered in this study. The same depth-dependent relationship has also recently been applied in thermal analyses of concrete gravity dams [31].

$$T_m(y) = c + (T_s - c)e^{-0.04y} \tag{18}$$

where $c = (T_b - T_s g)/(1 - g)$, $g = e^{-0.04H}$, T_b is the annual average temperature at the reservoir bottom, H is the reservoir depth (m), and the monthly average surface water temperature is given by $T_s = T_{am} + \Delta b$, where T_{am} is the local monthly average air temperature and Δb is the temperature increment.

Equation (18) is used to estimate the depth-dependent reservoir water temperature under the representative quasi-steady operating condition in January. The equation is applicable to seasonal or monthly mean thermal analyses when the vertical temperature distribution of the reservoir remains relatively stable, but is not intended to describe short-term transient water temperature responses induced by rapidly varying environmental or hydrodynamic conditions.

For the mechanical boundary conditions, an integral dam–foundation model is adopted. The bottom of the foundation is set as a fully constrained boundary, while the lateral boundaries are assigned normal constraints. In the stress field analysis, self-weight, hydraulic load, and thermal load are considered simultaneously. The low-temperature-induced thermal deformation is represented through thermal strain. The two-dimensional model was mainly used to investigate the temperature–stress distribution and local stress concentrations in the representative central section of the dam. Three-dimensional effects, including abutment constraints, transverse joints, outlet structures, and temperature variations along the dam axis, were not considered. In an actual dam, abutment constraints

may restrict deformation along the dam axis and generate additional out-of-plane stresses, while nonuniform temperature variations along the dam axis may induce longitudinal thermal stresses and spatial stress redistribution, thereby changing the magnitude and direction of local principal stresses and the locations of stress concentration. Therefore, the present results mainly represent the response of the representative central section rather than the complete three-dimensional stress state of the entire dam. Based on the above model and boundary conditions, the macro-scale temperature and stress fields of the dam during winter operation were first obtained. Local stress concentration regions were then identified, followed by meso-scale substitution analysis and comparison with the submodeling method.

3. Macroscopic Temperature Response Analysis of CSG Dam

3.1. Temperature Field Distribution During Winter Operation

Taking the low-temperature operating condition in January as the representative scenario, the temperature field of the cemented sand and gravel (CSG) dam during operation is numerically analyzed, as shown in Figure 4.

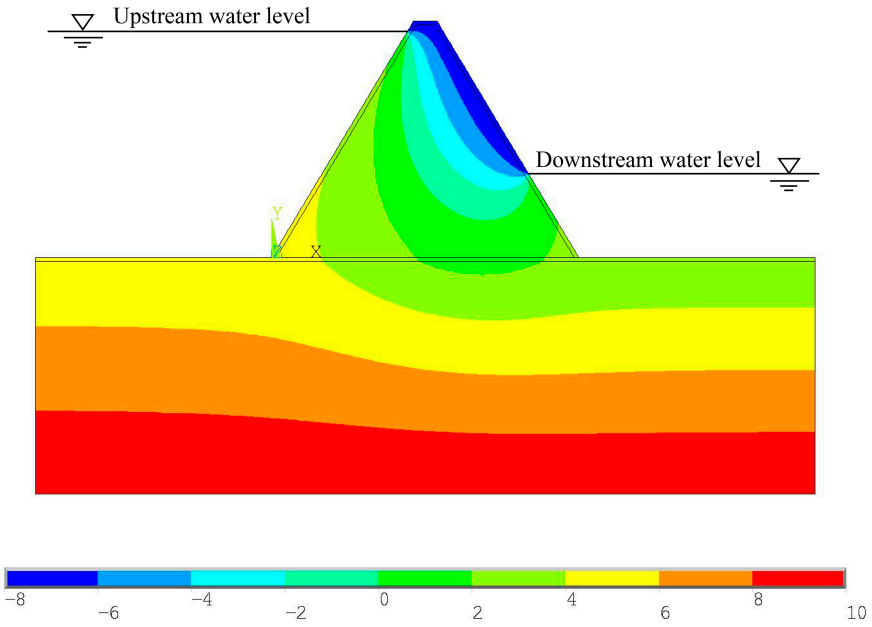

Figure 4. Quasi-steady temperature field in January (°C).

As illustrated in Figure 4, during winter low-temperature operation, the thermal effects of ambient air temperature and reservoir water temperature on the CSG dam are mainly concentrated near the surface, with a relatively shallow influence depth. The dam surface is directly exposed to cold air, causing the surface concrete to cool rapidly under ambient temperature, which leads to the development of significant temperature gradients in the near-surface region. In contrast, the interior and lower parts of the dam are jointly regulated by reservoir water temperature and the thermal inertia of the dam body, resulting in a relatively smooth temperature distribution. Furthermore, the temperature difference between the cold air and the relatively warmer reservoir water intensifies the temperature gradient near the upstream surface region.

Overall, the temperature field of the dam during winter operation exhibits a characteristic pattern of "pronounced variation at the surface and gradual variation in the interior." The influence of the low-temperature environment is primarily confined to the surface region, while its impact on deeper zones of the dam remains limited.

3.2. Thermal Stress Distribution During Winter Operation

The stress field of the cemented sand and gravel (CSG) dam under the low-temperature condition in January is analyzed, as shown in Figure 5.

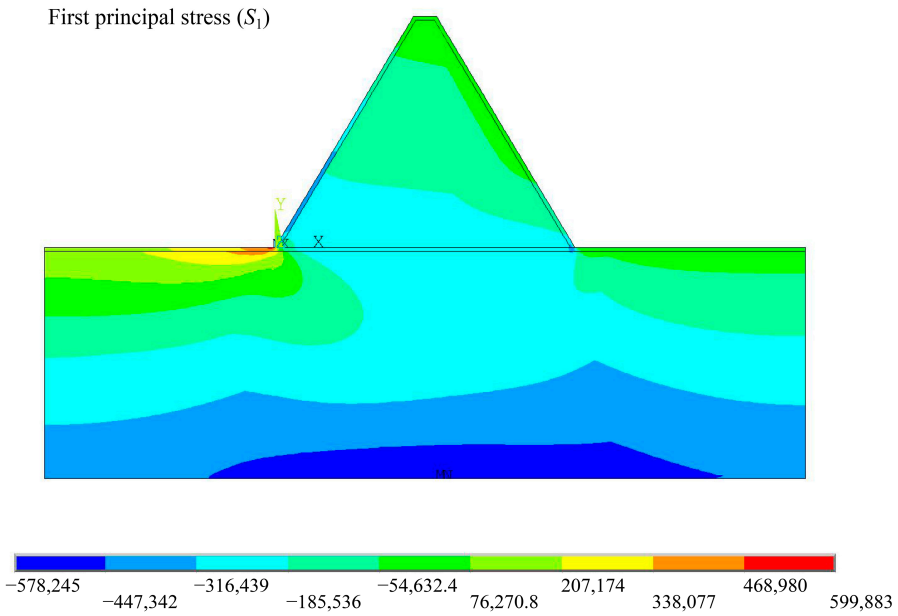

Figure 5. Stress contour in January with thermal load (Pa). MN indicates the location of the minimum first principal stress.

As illustrated in Figure 5, under the combined effects of self-weight, hydraulic load, and thermal load, the dam body is predominantly in a compressive stress state. The maximum tensile stress occurs at the upstream dam heel, while relatively large compressive stresses are observed at the downstream dam foundation region. The apparent discontinuity at the dam heel is a manifestation of localized stress concentration caused by the abrupt changes in geometry, material properties, and constraint conditions at the intersection of the upstream dam face and the dam–foundation interface, rather than a discontinuity in the finite element mesh or model connectivity. In addition, in the cushion layer at the dam–foundation interface, the tensile stress values are significantly higher than those in other parts of the dam, indicating a pronounced stress concentration in this region. In contrast, although relatively large temperature gradients occur near the downstream surface, the corresponding stress value is only 0.0763 MPa. This suggests that the thermal load induced by low-temperature conditions has a relatively limited influence on the overall stress field of the dam and mainly manifests as a local effect.

To further investigate the influence of the thermal load on the dam, an additional analysis was conducted without applying the thermal load, while the self-weight, hydrostatic pressure, and mechanical boundary conditions were kept unchanged. The resulting stress distribution is shown in Figure 6.

As shown in Figure 6, when the thermal load is excluded, the overall stress distribution of the dam remains generally consistent with that obtained under the January low-temperature condition, and the upstream dam heel remains the principal tensile stress concentration region. However, the maximum tensile stress increases from 0.60 MPa with the thermal load to 1.01 MPa without the thermal load. Because the exact peak locations differed slightly between the two cases, the node corresponding to the maximum first principal tensile stress in the case without thermal loading was selected for a fixed-location comparison, as shown in Table 3. The same mesh, mechanical loads, boundary conditions, result coordinate system, and nodal averaging settings were used for both cases.

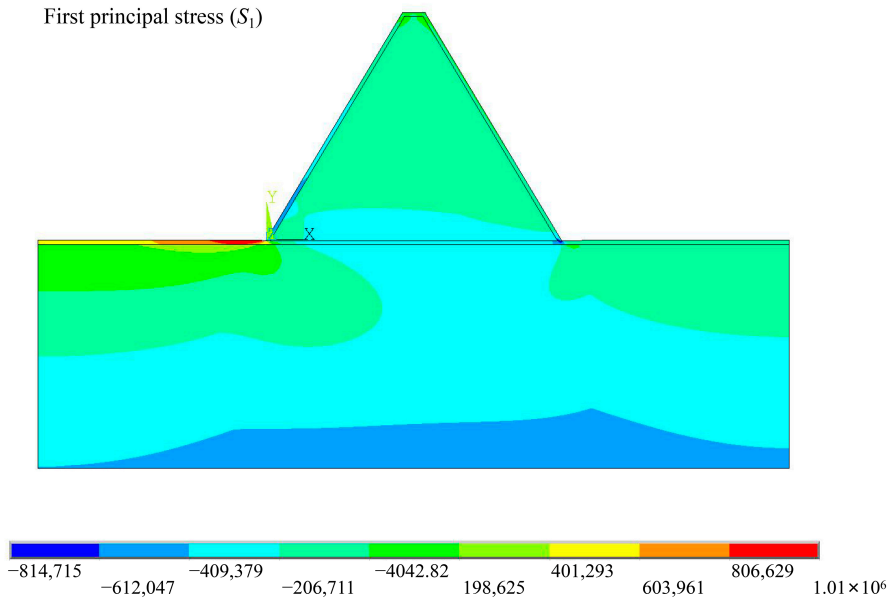

Figure 6. Stress contour in January without thermal load (Pa).

Table 3. Stress components at a fixed critical node near the upstream dam heel (MPa).

Loading Condition	S_X	S_Y	S_{XY}	S_1
Without thermal loading	1.001	−0.051	−0.096	1.010
With thermal loading	0.519	−0.019	−0.021	0.520

As shown in Table 3, after the thermal load was applied, the horizontal normal stress S_X at the fixed node decreased from 1.001 MPa to 0.519 MPa, while the absolute value of the shear stress S_{XY} decreased from 0.096 MPa to 0.021 MPa. Accordingly, the first principal tensile stress S_1 decreased from 1.01 MPa to 0.52 MPa. The reduction in S_1 at this location was mainly attributable to the decrease in the horizontal tensile stress component.

This difference mainly results from the differential thermal deformation induced by the non-uniform winter temperature field. The downstream face is more strongly affected by low air temperatures and therefore undergoes greater thermal deformation, whereas the upstream face is moderated by the reservoir water temperature and exhibits relatively smaller thermal deformation. Under foundation restraint, the differential thermal deformation between the upstream and downstream faces alters the local deformation compatibility and stress state near the upstream dam heel, reducing the magnitudes of the horizontal tensile stress and shear stress. Consequently, the first principal tensile stress decreases, while the overall distribution pattern of the first principal stress in the dam remains essentially unchanged.

Considering the allowable tensile strength of 1.78 MPa and the compressive strength of 25 MPa for the C25 concrete in the surface layer of the dam, the overall stress levels of the dam under both loading conditions remain below the corresponding material strength limits, indicating that strength failure is unlikely to occur under the investigated conditions within the linear–elastic framework.

4. Temperature Response Analysis of Two Local Analysis Methods

4.1. Local Meso-Scale Response Based on Adaptive Macro–Meso FEM

To determine an appropriate value for the principal tensile stress threshold in the adaptive macro–meso analysis, a comparative study of candidate element identification under different threshold values was conducted, as summarized in Table 4.

Table 4. Influence of principal tensile stress threshold on candidate element identification.

Principal Tensile Stress Threshold (MPa)	Number of Candidate Elements	Location of Candidate Elements	Upstream Dam Heel Identified
0.10	18	Surface region and near dam heel	No
0.15	6	Near upstream dam heel	Yes
0.20	2	Near upstream dam heel	Yes

Considering the extremely low tensile strength of the internal cemented sand and gravel, the principal tensile stress threshold was determined by referring to existing experimental results on CSG damming materials and relevant specification requirements. Previous studies showed that, when the water–binder ratio is 1.0–1.1, the splitting tensile strength of CSG damming materials can reach approximately 0.5–0.6 MPa [32]. In this study, 0.60 MPa was therefore adopted as the representative reference tensile strength of the cemented sand and gravel. According to the Design Specification for Concrete Gravity Dams (SL 319—2018) [33], the allowable stress of dam concrete should be determined by dividing the corresponding ultimate strength by the safety factor, and the tensile safety factor for local concrete regions with tensile requirements should not be less than 4.0. Based on the above tensile strength of the material and the safety factor specified in the design specification, the principal tensile stress threshold can be determined using Equation (19):

$$\sigma_{th} = \frac{f_t}{K} \tag{19}$$

where σ_{th} is the principal tensile stress threshold, f_t is the representative reference tensile strength of the cemented sand and gravel, and K is the tensile safety factor. Taking f_t = 0.60 MPa and K = 4.0, σ_{th} is obtained as 0.15 MPa. Therefore, 0.15 MPa was adopted as the principal tensile stress triggering threshold in the adaptive macro–meso analysis.

As shown in Table 4, when the threshold is 0.10 MPa, a relatively large number of candidate elements are identified, and their distribution is scattered. When the threshold is 0.20 MPa, the number of candidate elements is too small, resulting in insufficient representativeness. When the threshold is 0.15 MPa, the high-tensile-stress region near the upstream dam heel can be effectively identified, with a moderate number of candidate elements. Therefore, 0.15 MPa is consistent with the threshold estimated based on the representative reference tensile strength of the material and the safety factor specified in the design specification, and it can also satisfy the requirement for identifying local high-tensile-stress regions. Thus, it can be used as the triggering threshold for meso-scale analysis in this study.

When multiple CSG elements simultaneously satisfy the stress criterion, the element with the largest first principal tensile stress at its integration points is selected for meso-scale substitution. The corresponding results are shown in Figure 7. Figure 7a presents the macro-scale stress contour and highlights the macro-scale element selected for meso-scale substitution, whereas Figure 7b shows the stress contour of the corresponding meso-scale model after substitution.

As illustrated in Figure 7, under the strong constraints imposed by the foundation and internal concrete, the CSG region near the upstream dam heel exhibits tensile stress concentration at the macro scale. When this macro-scale tensile stress is transferred to the meso-scale model composed of aggregates and mortar, a pronounced stress redistribution occurs. Due to their higher stiffness, aggregates primarily bear compressive stresses, while tensile stress concentration develops in the mortar matrix and at the aggregate–mortar interfaces, with a maximum value of approximately 0.15 MPa. Since Figure 7b corresponds

to the selected local CSG element after the adaptive macro–meso transition, it mainly reflects the meso-scale stress redistribution within this critical local region.

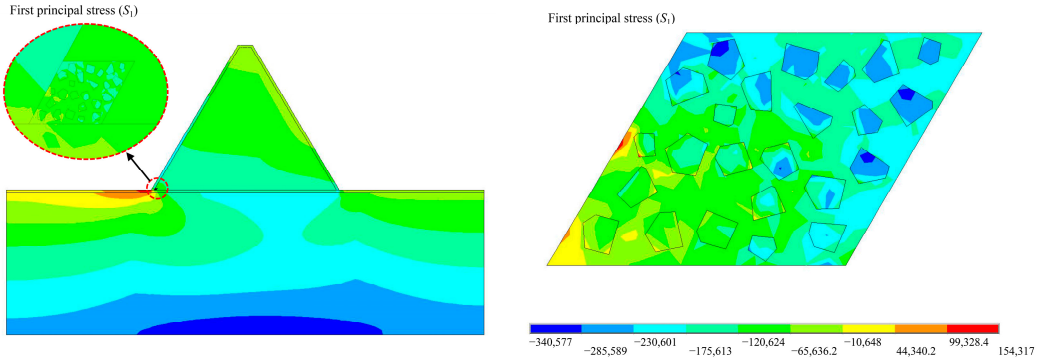

Figure 7. Adaptive macro–meso cross-scale stress distribution of CSG dam. (**a**) Macro–meso cross-scale stress contour. (**b**) Meso-scale stress contour corresponding to highlighted macro-scale element in (**a**) (Pa).

To evaluate the influence of random aggregate configurations on the meso-scale peak stress, ten random aggregate models were generated using different random seeds. The aggregate particle size range, gradation scheme, material parameters, loading conditions, and boundary conditions were kept identical for all models. The maximum first principal tensile stresses within the local meso-scale domains of the ten models were 0.1488, 0.1582, 0.1500, 0.1465, 0.1593, 0.1564, 0.1491, 0.1513, 0.1528, and 0.1521 MPa. The corresponding statistical results are presented in Table 5.

Table 5. Statistical results for the maximum first principal tensile stress of random aggregate models.

Number of Random Realizations N	Mean of the Maximum First Principal Tensile Stress E(X)/(MPa)	Standard Deviation S (MPa)	Coefficient of Variation C = S/E(X)
10	0.1525	0.0043	0.0279

The mean maximum first principal tensile stress of the ten models was 0.1525 MPa, with a sample standard deviation of 0.0043 MPa and a coefficient of variation of 0.0279. Although the specific locations of the peak stress points varied among the random configurations, they were all concentrated in the lower-left part of the local meso-scale region near the dam heel, while the overall peak stress level remained relatively stable.

The results indicate that, under thermal loading, the macro-scale tensile stress exhibits a nonuniform distribution after being transferred to the meso-scale structure. Across the ten random aggregate configurations, pronounced stress concentrations were observed near the aggregate–mortar interfaces, consistent with the stress distributions reported in previous studies on the thermal stress of CSG random aggregate models and macro–meso thermal damage in concrete gravity dams [34,35]. These results demonstrate that the adaptive macro–meso finite element method can effectively characterize the local stress redistribution within the selected element under a unified global computational framework.

4.2. Local Meso-Scale Response Based on Submodeling Method

To enable a direct comparison with the adaptive macro–meso finite element method presented in Section 4.1, the submodel region was defined as the macro-scale element selected for meso-scale substitution in the adaptive analysis. First, the global macro-scale analysis was performed under the combined effects of self-weight, hydrostatic pressure, and

thermal load. The nodal displacements along the cut boundary of the selected element were then interpolated from the global analysis results and prescribed as boundary conditions for the submodel. The submodel employed the same meso-scale geometry and material parameters as those used in the adaptive analysis. The corresponding mesh discretization is shown in Figure 8.

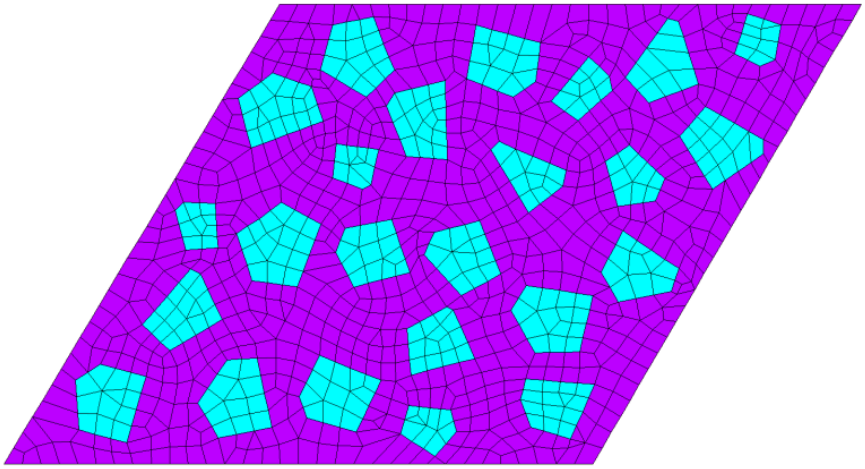

Figure 8. Mesh discretization of the submodel. The purple region represents the mortar matrix, while the cyan regions represent the aggregates.

The meso-scale stress distribution obtained from the submodeling method is presented in Figure 9.

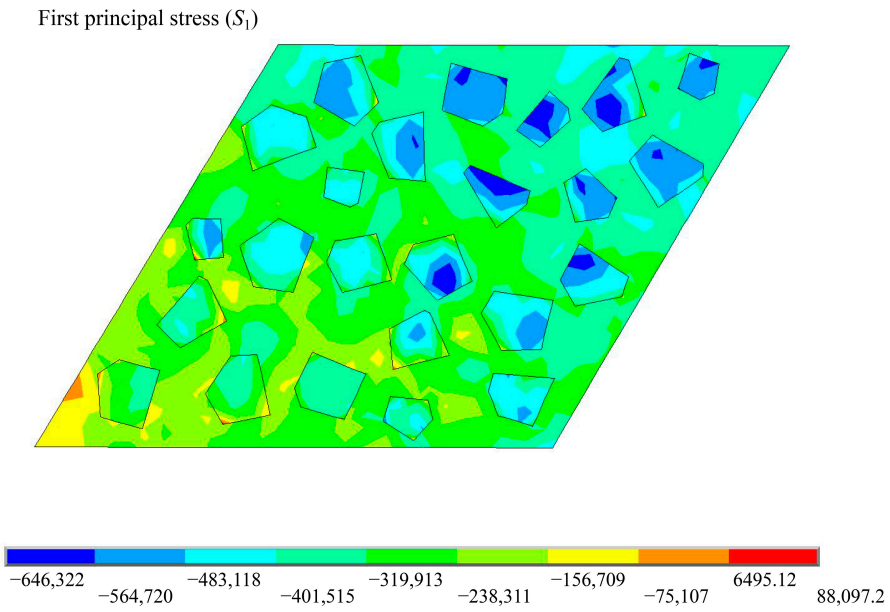

Figure 9. Meso-scale stress distribution obtained by the submodeling method (Pa).

As shown in Figure 9, after mapping the displacement results from the global model onto the boundary of the submodel, the meso-scale region is predominantly subjected to compressive stress, with a maximum compressive stress of 0.65 MPa. Due to the differences in material properties between aggregates and mortar, local tensile stress concentration occurs near the interfaces, with a peak value of 0.09 MPa.

The results indicate that, under the displacement boundary constraints derived from the global model, significant meso-scale stress redistribution still exists within the submodel. In particular, the aggregate–mortar interface is identified as the primary region of tensile

stress concentration. Compared with the adaptive macro–meso finite element method, the submodeling method yields a lower peak tensile stress; however, both approaches consistently indicate that the interface region is critical and requires particular attention.

4.3. Method Comparison and Mechanism Discussion

In this study, the same meso-scale geometric model and material parameters are adopted to compare the meso-scale mechanical responses of CSG material elements using the adaptive macro–meso finite element method (FEM) and the submodeling method. The results are shown in Figure 10.

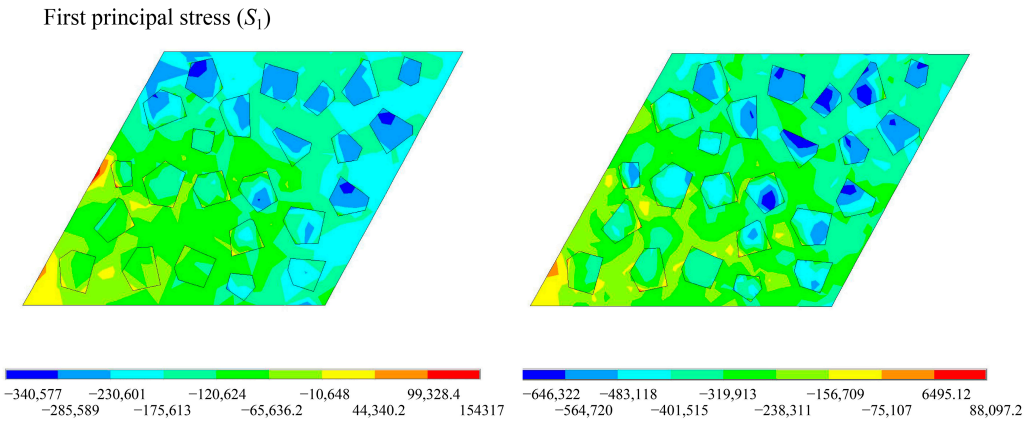

Figure 10. Meso-scale stress comparison (Pa): adaptive macro–meso finite element method (**left**) and submodeling method (**right**).

As shown in Figure 10, the peak tensile stresses obtained using the adaptive macro–meso FEM and the submodeling method are 0.15 MPa and 0.09 MPa, respectively, corresponding to an absolute difference of 0.06 MPa. Although the two methods identify similar stress-concentration locations and overall stress-distribution patterns, a certain difference remains in the peak tensile stress.

This difference may be related to the distinct boundary-transfer mechanisms adopted by the two methods. In the adaptive macro–meso FEM, the meso-scale elements participate directly in the assembly and solution of the global stiffness matrix. In contrast, the submodeling method applies the displacement field obtained from the macro-scale model as the cut-boundary condition for an independent local analysis.

From a meso-scale mechanical perspective, the macro-scale tensile stress near the upstream dam heel is transferred to the heterogeneous aggregate–mortar structure, where deformation incompatibility arises due to material property differences. Aggregates, with higher stiffness, primarily carry compressive stresses, while tensile stress concentration tends to develop in the mortar matrix and particularly at the aggregate–mortar interfaces. Therefore, although the two methods differ in peak stress magnitude, they consistently identify the same critical high-stress regions.

Overall, the two methods identify similar meso-scale stress concentration locations and general distribution patterns, with relatively high tensile stresses occurring mainly near the aggregate–mortar interfaces. Overall, the submodeling results provide an independent qualitative comparison for the local analysis results obtained from the proposed adaptive macro–meso FEM. However, because the peak tensile stresses obtained using the two methods differ by 0.06 MPa and no exact reference solution is available, the present comparison does not constitute a quantitative validation of accuracy. Further assessment should be based on full-field meso-scale simulations, experimental data, or field-monitoring results.

5. Conclusions

This study investigates the cross-scale temperature response of cemented sand and gravel (CSG) dams and proposes an adaptive macro–meso finite element method triggered by a principal tensile stress threshold. Based on the macro-scale calculation, local high-stress regions are replaced by meso-scale models, and the macro–meso scale transition is achieved through coordinated local mesh refinement. The Shoukoubao CSG dam is taken as an engineering case, and the following conclusions are obtained:

(1) Under winter low-temperature conditions, the temperature difference between the interior and exterior of the dam increases, and certain tensile stresses appear near the dam surface. However, thermal stress is not the main factor affecting the overall stress state of the dam, while hydraulic load still plays a dominant role.

(2) Within the macro–meso multiscale finite element framework, local meso-scale analysis is achieved through meso-scale substitution and mesh reconstruction of local high-stress elements. The proposed method can identify high-tensile-stress regions, such as the upstream dam heel, and reveal stress redistribution among aggregates, mortar, and their interfaces, where stress concentrations tend to occur. For the ten random aggregate models, the mean and standard deviation of the maximum first principal tensile stress were 0.1525 MPa and 0.0043 MPa, respectively, indicating that the results were generally stable.

(3) Comparison with the submodeling method shows that the two methods exhibit good consistency in local stress distribution patterns and identification of high-stress regions. The submodeling results provide an independent qualitative comparison for the local analysis results obtained by the proposed adaptive macro–meso finite element method and offer a reference for cross-scale analysis of the temperature response of CSG dams.

In this study, only local high-stress regions are selected for meso-scale replacement analysis, and full-field meso-scale simulations, experimental data, or field-monitoring results are currently unavailable as exact references. Therefore, the present comparison does not constitute a strict quantitative validation. Future studies will further evaluate the applicability and computational accuracy of the proposed method using larger sets of random aggregate realizations, full-field meso-scale simulations, and measured data.

Author Contributions: Conceptualization, L.Z. and Y.Z.; Methodology, L.Z. and Y.Z.; Software, Y.Z.; Validation, L.Z., Y.Z. and L.G.; Formal Analysis, L.Z.; Investigation, Y.Z. and J.Z.; Resources, L.G.; Data Curation, L.Z. and J.Z.; Writing—Original Draft Preparation, L.Z. and Y.Z.; Writing—Review & Editing, L.Z., Y.Z., L.G. and J.Z.; Visualization, L.Z.; Supervision, Y.Z.; Project Administration, Y.Z.; Funding Acquisition, L.G. All authors have read and agreed to the published version of the manuscript.

Funding: This research was funded by the National Natural Science Foundation of China, grant number 52109154.

Institutional Review Board Statement: Not applicable.

Informed Consent Statement: Not applicable.

Data Availability Statement: All data included in this paper are available upon request by contacting the corresponding author.

Conflicts of Interest: The authors declare no conflicts of interest.

References

1. Jia, J.; Lino, M.; Jin, F.; Zheng, C. The Cemented Material Dam: A New, Environmentally Friendly Type of Dam. *Engineering* **2016**, *2*, 490–497. [CrossRef]
2. Cai, X.; Zhang, Y.; Guo, X.; Zhang, X.; Li, F.; Zhang, T. Review on research progress of cemented sand and gravel dam. *Sci. Eng. Compos. Mater.* **2022**, *29*, 438–451. [CrossRef]

3. Jia, J.; Ding, L.; Wu, Y.; Zhao, C.; Zhao, L. Research and application of key technologies for the construction of cemented material dam with soft rock. *Appl. Sci.* **2023**, *13*, 4626. [CrossRef]
4. Jiang, M.; Cai, X.; Guo, X.; Liu, Q.; Zhang, T. Adiabatic temperature rise test of cemented sand and gravel (CSG) and its application to temperature stress prediction of CSG dam. *Adv. Mater. Sci. Eng.* **2020**, *2020*, 3898391. [CrossRef]
5. Mirković, U.; Kuzmanović, V.; Todorović, G. Long-term thermal stress analysis and optimization of contraction joint distance of concrete gravity dams. *Appl. Sci.* **2022**, *12*, 8163. [CrossRef]
6. Rodrigues, E.A.; Manzoli, O.L.; Bitencourt, L.A.G.; Bittencourt, T.N.; Sánchez, M. An adaptive concurrent multiscale model for concrete based on coupling finite elements. *Comput. Methods Appl. Mech. Eng.* **2018**, *328*, 26–46. [CrossRef]
7. Sun, B.; Li, Z. Adaptive mesh refinement FEM for seismic damage evolution in concrete-based structures. *Eng. Struct.* **2016**, *115*, 155–164. [CrossRef]
8. Sun, B.; Li, Z. Adaptive concurrent three-level multiscale simulation for trans-scale process from material mesodamage to structural failure of concrete structures. *Int. J. Damage Mech.* **2016**, *25*, 750–769. [CrossRef]
9. Xu, L.; Jiang, L.; Shen, L.; Gan, L.; Dong, Y.; Su, C. Adaptive hierarchical multiscale modeling for concrete trans-scale damage evolution. *Int. J. Mech. Sci.* **2023**, *241*, 107955. [CrossRef]
10. Xu, L.; Jiang, L.; Wang, S.; Ren, Q. An adaptive macro-meso progressive analysis method for cross-scale damage and cracking of concrete. *J. Southeast Univ. Nat. Sci. Ed.* **2022**, *52*, 1052–1062.
11. Unger, F.J.; Eckardt, S. Multiscale Modeling of Concrete: From Mesoscale to Macroscale. *Arch. Comput. Methods Eng.* **2011**, *18*, 341–393. [CrossRef]
12. Rezakhani, R.; Zhou, X.; Cusatis, G. Adaptive multiscale homogenization of the lattice discrete particle model for the analysis of damage and fracture in concrete. *Int. J. Solids Struct.* **2017**, *125*, 50–67. [CrossRef]
13. Barbhuiya, S.; Jivkov, A.; Das, B.B. A review of multi-scale modelling of concrete deterioration: Fundamentals, techniques and perspectives. *Constr. Build. Mater.* **2023**, *406*, 133472. [CrossRef]
14. Zhu, B. *Temperature Stress and Temperature Control of Mass Concrete*; China Water & Power Press: Beijing, China, 2012.
15. Guo, L.; Luo, G.; Zhong, L.; Chen, S. Simulation of freeze-thaw damage of hydraulic concrete structures during construction. *Trans. Chin. Soc. Agric. Eng.* **2012**, *28*, 82–87. [CrossRef]
16. Li, Z.; Liang, X.; Liu, C.; Liang, M.; van Breugel, K.; Ye, G. Thermal deformation and stress of alkali-activated slag concrete under semi-adiabatic condition: Experiments and simulations. *Cem. Concr. Res.* **2022**, *159*, 106887. [CrossRef]
17. Zhang, J.; Zhou, D.; He, X.; Hu, X.; Qiang, S. Comparative analysis of temperature and stress simulations in mass concrete for sluice gate structures based on Chinese and American standards. *Materials* **2025**, *18*, 100. [CrossRef] [PubMed]
18. Zhang, Y.; Pan, J.; Sun, X.; Feng, J.; Sheng, D.; Wang, H.; Zhou, X.; He, Y.; Diao, M.; Zhan, Q. Simulation of thermal stress and control measures for rock-filled concrete dam in high-altitude and cold regions. *Eng. Struct.* **2021**, *230*, 111721. [CrossRef]
19. Yang, S.; Yuan, S. Comparative analysis of several adaptive finite element methods. *Eng. Mech.* **2025**, *42*, 1–8. [CrossRef]
20. Gierden, C.; Kochmann, J.; Waimann, J.; Svendsen, B.; Reese, S. A review of FE-FFT-based two-scale methods for computational modeling of microstructure evolution and macroscopic material behavior. *Arch. Comput. Methods Eng.* **2022**, *29*, 4115–4135. [CrossRef]
21. Mori, T.; Tanaka, K. Average stress in matrix and average elastic energy of materials with misfitting inclusions. *Acta Metall.* **1973**, *21*, 571–574. [CrossRef]
22. Guo, L.; Zhong, L.; Zheng, C.; Guo, L.; Wang, L. Damage and failure study of recycled concrete containing bricks based on improved random aggregate model. *J. Basic Sci. Eng.* **2019**, *27*, 1390–1398. [CrossRef]
23. Zhuo, J.; Zhang, Y.; Ma, M.; Zhang, Y.; Zheng, Y. Uniaxial compression failure and size effect of recycled aggregate concrete based on meso-simulation analysis. *Materials* **2022**, *15*, 5710. [CrossRef] [PubMed]
24. Li, H.; Fu, S.; Li, G.; Hu, G. FEA of effects induced by diurnal temperature variation on downstream surface of Xiaowan Arch Dam. *Adv. Civ. Eng.* **2021**, *2021*, 6300387. [CrossRef]
25. Freitas, M.; Ben Ftima, M.; Léger, P.; Bouaanani, N. Three-dimensional failure envelope of concrete dam shear keys. *Eng. Struct.* **2022**, *269*, 114766. [CrossRef]
26. Song, L.; Wu, M.; Wang, J.; Xu, Y. Seismic damage analysis of the outlet piers of arch dams using the finite element sub-model method. *Earthq. Eng. Eng. Vib.* **2016**, *15*, 617–626. [CrossRef]
27. Yin, Y.; Ren, Q. Macro-meso damage and failure analysis of concrete gravity dams under seismic action based on submodel method. *Eng. Mech.* **2024**, *41*, 15–22, 82. [CrossRef]
28. Fu, Y. Seepage Characteristics and Temperature-Control Simulation of Cemented Sand and Gravel Dams. Master's Thesis, North China University of Water Resources and Electric Power, Zhengzhou, China, 2021. [CrossRef]
29. Cai, X.; Jiang, M.; Guo, X.; Chen, J.; Zhao, Q. Experimental study on the creep behaviour of cemented sand and gravel (CSG) and temperature stress prediction of CSG dam under seasonal temperature change. *Adv. Civ. Eng.* **2020**, *2020*, 8289520. [CrossRef]
30. Zhu, B. Prediction of Water Temperature in Deep Reservoirs. *Dam Eng.* **1997**, *8*, 13–25.

31. Liang, W.; Leng, L.; Tian, H.; Tian, X.; Zhang, C. Cause Investigation of Fractures in the Anti-Arc Portion of the Gravity Dam's Overflow and the Top of the Substation Tunnel. *Buildings* **2023**, *13*, 1531. [CrossRef]
32. Wang, R.; Gong, A.; Shao, S.; Qu, B.; Xu, J.; Wang, F.; Liu, F. Microscopic analysis of cementitious sand and gravel damming materials. *Fluid Dyn. Mater. Process.* **2024**, *20*, 749–769. [CrossRef]
33. *SL 319-2018*; Design Code for Concrete Gravity Dams. China Water & Power Press: Beijing, China, 2018.
34. Jiao, Y.; Cheng, L.; Wang, N.; Wang, S.; Ma, L. Calculation and analysis of temperature damage of Shimantan concrete gravity dam based on macro–meso model. *Materials* **2022**, *15*, 7138. [CrossRef] [PubMed]
35. Guo, L.; Liang, T.; Zhong, L. Early age temperature effect of cemented sand and gravel based on random aggregate model. *Sci. Eng. Compos. Mater.* **2025**, *32*, 20250059. [CrossRef]